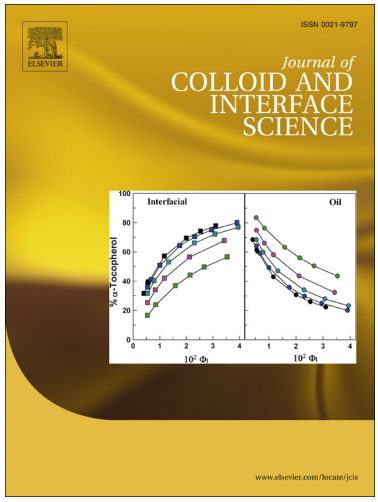

On the phase-field modelling of a miscible liquid/liquid boundary

Ruilin Xie, Anatoliy Vorobev

PII: S0021-9797(15)30336-2
DOI: http://dx.doi.org/10.1016/j.jcis.2015.11.026
Reference: YJCIS 20877

To appear in: *Journal of Colloid and Interface Science*

Please cite this article as: R. Xie, A. Vorobev, On the phase-field modelling of a miscible liquid/liquid boundary, *Journal of Colloid and Interface Science* (2015), doi: http://dx.doi.org/10.1016/j.jcis.2015.11.026

On the phase-field modelling of a miscible liquid/liquid boundary

Ruilin Xie, Anatoliy Vorobev*

[a] *Energy Technology Research Group, Faculty of Engineering and the Environment, University of Southampton, Southampton SO17 1BJ, UK*

Abstract

Mixing of miscible liquids is essential for numerous processes in industry and nature. Mixing, i.e. interpenetration of molecules through the liquid/liquid boundary, occurs via interfacial diffusion. Mixing can also involve externally or internally driven hydrodynamic flows, and can lead to deformation or disintegration of the liquid/liquid boundary. At the moment, the mixing dynamics remains poorly understood. The classical Fick's law, generally accepted for description of the diffusion process, does not explain the experimental observations, in particular, the recent experiments with dissolution of a liquid solute by a liquid solvent within a horizontal capillary [1]. We present the results of the numerical study aimed at development of an advanced model for the dissolution dynamics of liquid/liquid binary mixtures. The model is based on the phase-field (Cahn-Hilliard) approach that is used as a physics-based model for the thermo- and hydrodynamic evolution of binary mixtures. Within this approach, the diffusion flux is defined through the gradient of chemical potential, and, in particular, includes the effect of barodiffisuon. The dynamic interfacial stresses at the miscible interface are also taken into account. The simulations showed that such an approach can accurately reproduce the shape of the solute/solvent boundary, and some aspects of the diffusion dynamics. Nevertheless, all experimentally-observed features of the diffusion motion of the solute/solvent boundary, were not reproduced.

Keywords: Miscible liquids, Diffusive interface, Non-Fickian diffusion, Dynamic surface tension, Cahn-Hilliard approach

*Anatoliy Vorobev

Email addresses: rx3c13@soton.ac.uk (Ruilin Xie), A.Vorobev@soton.ac.uk (Anatoliy Vorobev)

1. Introduction

It is known that the rate of diffusion of weak impurities in liquids is well defined by the classical Fick's law, i.e. with the gradient flux linearly proportion to the gradient of concentration. It is also known that this simple approach is not valid for the case of large concentration gradients, in particular, for the description of diffusion at a liquid/liquid (solute/solvent) boundary. This, in particular, was illustrated by the recent experiments, where mixing of liquid solute and liquid solvent was investigated [1]. The settings of the experiments were rather simple: a long capillary, initially saturated with one liquid (solute), was immersed horizontally into a solvent-filled thermostatic bath. The tube's diameters varied from 0.2mm to 1.6mm. Both ends of the tube were open, and no pressure gradients between the tube ends were applied. The experiments were conducted with different liquids, in particular, with the glycerol/water and soybean oil/hexane binary mixtures which are miscible in any proportions. Following the common expectations one would assume that the solute/solvent boundaries should remain stationary (if there are no mechanisms for the hydrodynamic flows) and would just slowly smear in time. Contrary to this, two solute/solvent boundaries were seen at the sides of the capillary for very long time periods. The interfaces were moving towards the middle of the tube with the speed that was considerably higher than the rate of interface smearing. The speed of the interface movement depended on time as $t^{-1/3}$ in the beginning and $t^{-2/3}$ in the later moments. In addition, it was observed that the interface should be endowed with the surface tension, since its inclined shape should be described by the balance of the capillary and gravity forces. The rate of interface propagation was found to depend on the tube's diameter, so the dissolution occurred slower in the tubes of smaller diameters. The speed of the interface movement did not depend on the shape of the tube's cross section and on the tube's length. The convective flows were found negligible, and thus the evolution of the interfaces was suggested to be primarily diffusion-driven.

In the current work, we aim to develop a theoretical model capable of reproducing this behaviour. We start with the use of the classical Fick's law with however the diffusion coefficient that strongly depends on concentration. Strictly speaking, this approach does not distinguish the phases, but the concentration dependence of the diffusion coefficient permits modelling of sharper diffusion fronts. After that, we introduce the concept of interface by adopting the phase-field approach.

Currently, the phase-field approach is mostly used as a numerical tool for tracing immiscible interfaces [2, 3, 4, 5]. In the current work, however, this approach is used as a comprehensive physical

model capable of describing the thermo- and hydrodynamic evolution of multiphase binary mixtures with undergoing phase transformations. Within the phase-field model, the diffusion process is defined through the gradient of the chemical potential, taking into account the effect of barodiffusion [6, 7]. This model also captures the surface tension effects existent at miscible boundaries, thus permitting us to model the inclined shape of the solute/solvent boundary. Finally, we also add the hydrodynamics to investigate its possible role in the mixing of two liquids confined into a capillary.

The importance of the surface tension effects for miscible interfaces was first emphasized by Korteweg and van der Walls, who suggested that these effects can be mimicked by gradients of concentration [8]. Cahn and Hilliard [9, 10] proposed to define the free energy as a function of not only concentration but also of the concentration gradient, adding a term that takes into account the surface tension effects. They used this approach primarily to model the dynamics of phase transitions in solids [11, 4]. Later, the same idea was used to define the phase transitions in liquids, and the full equations for the thermo- and hydrodynamic evolution of liquid/liquid binary mixtures were derived by Lowengrub and Truskinovsky [12]. The resultant Cahn-Hilliard-Navier-Stokes equations were hardly feasible for the numerical treatment mostly due to the necessity to use the full continuity equation because the mixture density is in general a function of concentration. Later, on the basis of the multiple-scale method, the quasi-acoustic effects were filtered out, so the Boussinesq approximation of the full equations was obtained [6].

Some features of the Cahn-Hilliard-Navier-Stokes equations were earlier used in different numerical studies. For instance, a model that takes into account the Korteweg force but assumes that diffusion is still driven by the simple Fick's law was used to simulate the miscible displacement of one liquid by another from a capillary [13, 14, 15]. The consideration was however limited for a rather fast process at very high Peclet numbers, when the effect of diffusion was negligible. The similar approach was used to study the spreading of the interface boundary and generation of the convective motion near the boundary by the action of the Korteweg force [16, 17].

The evolution of a miscible droplet immersed into a another liquid that is enclosed into capillary and subjected to axial rotation (the configuration of the spinning droplet tensiometry) was experimentally studied in Ref. [18], where the existence of the dynamic surface tension at a miscible interface was confirmed. The spreading of a miscible interface in a vertical cuvette was experimentally studied in Ref. [19], where it was noted that the rate of interface spreading does not obey the Fick's law. For the mixture of 1-butanol/water, the spreading rate was proportional to

$t^{0.09}$, and the spreading occurred into the component not saturated with other component. For the isobutyric acid/water mixture in the conditions above the critical point (when both liquids are miscible in all proportions), the spreading occurred with the rate $t^{0.06}$ into the direction of the isobutric-acid-rich phase. In another work by the same group [20], it was found that the spreading of the monomer/polymer boundary obeys the Fick's law but only after some transitionary period that lasted for upto 30-60 minutes. The latter experiments were fulfilled with the low molecular weight polymers.

The theoretical modelling of the diffusive dissolution of a small droplet enclosed in a capillary was conducted by Ugrozov et al. [21]. In their work, the process of dissolution was split into two separate steps. During the first step, that was assumed to be infinitely short, the concentration within the droplet adjusted the saturation level. The concentration tails were formed in the medium surrounding the droplet. It was assumed that the dissolution of the droplet (i.e. its shrinkage) occurred due to Fickian diffusion happening at the concentration tails. This Fickian diffusion was the long second step of the dissolution process. No experimental verification of this theory was reported.

To conclude this introductory section, we wish to mention that a proper understanding of how the diffusion at the solute/solvent boundary occurs is of great practical importance. This is needed for accurate modelling of the mixing of chemicals in various chemical engineering processes, where such a mixing is required prior to chemical reactions occur. The dynamics of the solute/solvent mixtures enclosed into capillaries is important for modelling of such processes as vegetable solvent extraction (when the solvent is used to wash out the solute from the vegetable-based porous media), aquifer remediation (e.g. pumping of solute through contaminated soils), and enhanced oil recovery based on the miscible displacement and CO_2 sequestration [22, 23, 24, 25].

2. Fick's law results

We aim to reproduce the evolution of a binary mixture that saturates a horizontal capillary with open ends. The idea to investigate the diffusion within the capillary was discussed in [8], where such a configuration was suggested with a hope to obtain a simple-to-model $1D$ diffusion process. The experimental results of e.g. Ref. [1] clearly point out that the evolution of the solute/solvent mixture in the tube is much more complex, and could not be reduced to the $1D$ process.

Let us first prove that the Fick's law is not capable of describing the experimental observations of Ref. [1]. The Fick's equation reads

$$\frac{\partial C}{\partial t} = \nabla \cdot (D(C)\nabla C)\,. \tag{1}$$

This equation is written here in the non-dimensional form. Here, C is the concentration that is defined as the mass fraction of solute in a mixture, t is time, and $D(C)$ is the diffusion coefficient. We will model the evolution of the mixture in a plane layer defined by two coordinates x (along the layer) and y (across the layer). To non-dimensionlise eq. (1), the length of the layer was chosen as the length scale, L_*. The non-dimensional layer's height is denoted by L_y. Time in eq. (1) is non-dimensionalised with $\tau = L^2/D_0$, where D_0 is the typical value of the diffusion coefficient, e.g. the diffusion coefficient in pure solvent.

The coefficient of mutual diffusion $D(C)$ is in general a function that depends on concentration. For instance, for the glycerol/water mixture, the measurements of the mutual diffusion coefficient at 20^0C are reported in Ref. [26]. The formula that fits the measurements is

$$D(C) = 1.6 \cdot 10^{-10}(1 - 0.895C) \quad [m^2 \cdot s^{-1}]. \tag{2}$$

Thus, the rate of diffusion in pure glycerol is much lower, with the diffusion coefficient one order less than the diffusion coefficient for the pure water phase.

Figure 1a shows the $2D$ concentration fields in a single capillary for the concentration-dependent diffusion coefficient (2). We assume that the capillary is initially saturated with the solute and then the solvent penetrates from the open ends. Thus, initially $C = 1$ in the tube, and at the left and right boundaries we assume that $C = 0$. At the lower and upper plate, the boundary conditions impose no diffusion through the wall (zero normal derivative of concentration at the wall).

From the obtained results one sees that the solute/solvent boundaries are very diffusive, so it is rather difficult to position the interface. The penetration of the solvent can be characterised with the total mass of the solvent in the tube, that we define as

$$m = \frac{1}{L_y}\int_0^1 (1 - C)dV. \tag{3}$$

The resultant lines are shown in figures 1d,e (dash-dot-dot lines). The rate of diffusion (or the rate of solvent penetration) is time dependent, and it follows the classical $t^{1/2}$ dependence. The $1D$ and $2D$ results would obviously coincide, since there is no dependence on the vertical coordinate (and on the height of the plain layer).

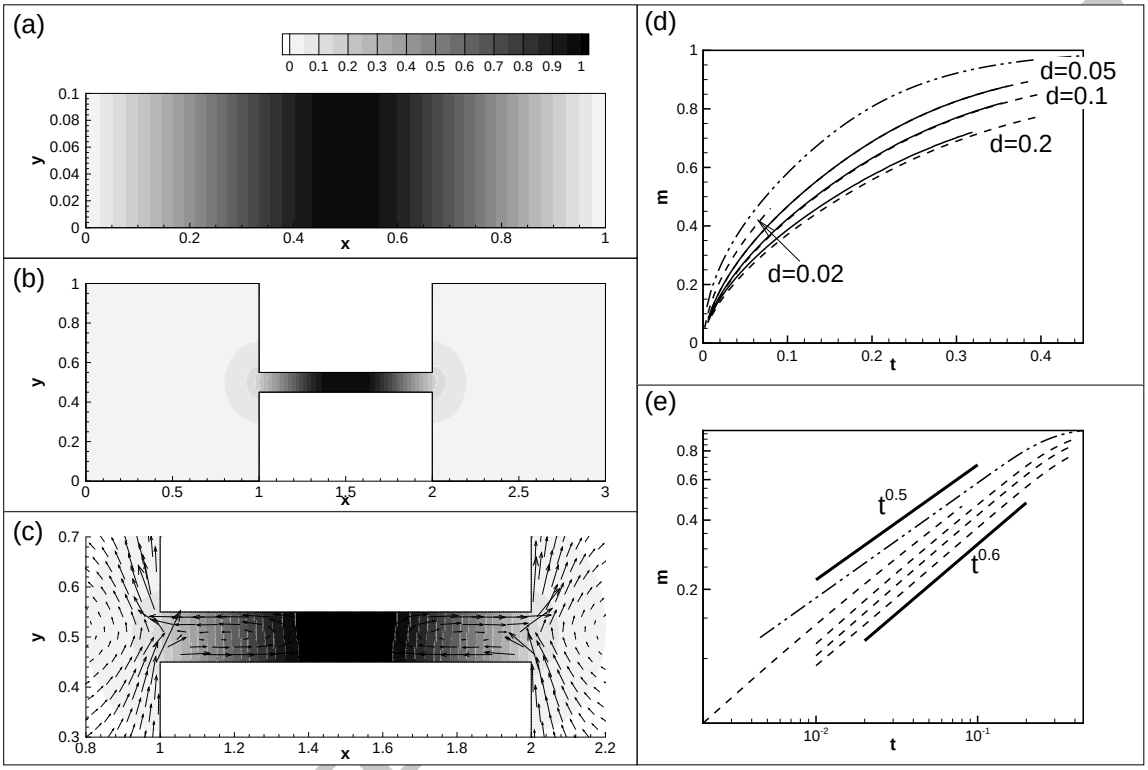

Figure 1: The Fickian evolution of the solute/solvent mixture. (a-c) The snapshots of the concentration and velocity fields at $t = 0.06$, (a) the results are obtained for the single capillary tube; (b) for the block geometry without hydrodynamic effects ($Gr = 0$); and (c) for the block geometry with account of the solutal convection ($Re = 10^{-4}$, $Gr = 10^{9}$). (d) The mass of the solvent that penetrates into the tube as a function of time. The dash-dot-dot line depicts the results for the single tube, the dashed lines show the data obtained for the block geometry without convection, and the solid lines with convection. The data for the block geometry is obtained for different tube diameters as depicted in the figure. (e) The data shown in (d) is replotted in the logarithmic coordinates. For clarity, only the curves obtained for the pure diffusive calculations are shown. The thick lines show the referral dependences.

Next, these simulations were repeated for the more sophisticated geometry, that included two big blocks, initially filled with the solvent, connected by the solute-filled tube. Such a geometry should be a closer reproduction of the experiment [1], and, in addition, such a geometry would allow us to introduce the flows (as otherwise the velocity boundary conditions at the capillary ends are difficult to define). The solutal convection is driven by gravity and by the dependence of the mixture density on concentration. For most of the liquids the density contrast between two liquids, ϕ, is small, so the density of the mixture can be approximately defined by the following linear formula

$$\rho = \rho_1(1 + \phi C), \quad \phi \equiv \frac{\rho_2 - \rho_1}{\rho_1}. \tag{4}$$

Here ρ_1 and ρ_2 are the densities of the pure mixture components.

The governing equations of the solutal convection are then defined by the equations that reflect the conservations of mass, momentum and species,

$$\nabla \cdot \vec{v} = 0, \tag{5}$$

$$\frac{\partial \vec{v}}{\partial t} + (\vec{v} \cdot \nabla)\vec{v} = -\nabla p + \frac{1}{Re}\nabla^2 \vec{v} - GrC\vec{\gamma}, \tag{6}$$

$$\frac{\partial C}{\partial t} + (\vec{v} \cdot \nabla)C = \nabla \cdot (D(C)\nabla C)\,. \tag{7}$$

These equations are written in standard notations, in non-dimensional form. Namely, $\vec{v}$ is the vector of velocity, p is the pressure, and $\vec{\gamma} = -\vec{g}/g$ is the unit vector directed upwards, where $\vec{g}$ is the gravitational acceleration. For the non-dimensionalisation, the diffusive time scale was used, $\tau = L^2/D_0$, as well as the following scales for velocity and pressure, L/τ and $\rho_1(L/\tau)^2$. The non-dimensional parameters entering the above equations are the Reynolds number[1]

$$Re = \frac{\rho_1 L^2}{\eta\tau} = \frac{\rho_1 D_0}{\eta}, \tag{8}$$

and the Grashoff number,

$$Gr = \phi\frac{g\tau^2}{L} = \phi\frac{gL^3}{D_0^2}. \tag{9}$$

[1]The definitions for these non-dimensional parameters are different from the standard ones, and the Reynolds number can be also interpreted as the inverse Schmidt number. The standard names are used as these two parameters appear in fronts of the corresponding terms of the governing equations, and continue to characterise the roles of the viscous and buoyancy forces.

The estimations of these parameters for the glycerol/water mixture give very small Reynolds numbers, $\sim 10^{-4}$, and very large Grashoff numbers, $\sim 10^{17}$. In our simulations, we were able to obtain the results for the Grashoff numbers up to $\sim 10^{10}$. At higher numbers, the induced hydrodynamic flows become so strong that the concentration field becomes non-physical with the values below 0 (which corresponds to a pure solvent) and above 1 (a pure solute).

For the calculations, we assume that the block geometry is enclosed by rigid walls. At all walls, we impose the no-slip boundary conditions for the velocity, and the no-penetration conditions for the diffusive flux (i.e. zero normal derivative of concentration).

The equations were solved numerically in the vorticity-streamfunction notations with the use of the finite-difference approach.

The snapshots of the concentration and velocity fields are depicted in figure 1b,c. The profiles look similar to what was obtained for the single tube. We found however that the dissolution occurs slower and with the different time dependence, which is closer to $t^{0.6}$ (see figures 1d,e). The slower dissolution is obviously explained by accumulation of the solute near the tube ends, which blocks the access of the fresh solvent. In the results obtained for the block geometry, we also observed some dependence on the tube's diameter: stronger solute levels are found near the ends of the tubes with larger diameters, which results in stronger reduction of the solvent penetration rates into the tube. This can be seen in figures 1d,e, where the dissolution from smaller tubes happen faster. Such a dependence contradicts to the experimental observations [1], where the dissolution in smaller tubes occurred slower.

In addition, we considered the effect of convection on the speed of the solvent penetration into the tube. Clearly, the convective flow should partially remove the solute from the tube ends transporting it either to the top or bottom of the containers (depending on which liquid is heavier). This in particular can be seen for the curve obtained for the tube with $d = 0.2$. For the smaller tubes the effect of convection was negligible, so the obtained curves were indistinguishable from the results for the pure diffusion calculations with $Gr = 0$.

Thus, modelling of the solvent penetration in the capillary on the basis of the simple Fick's law produces too diffusive solute/solvent boundary, and its experimentally-observed curved shape cannot be reproduced. An assumption that the dissolution is a purely diffusion process seems reasonable (however, it was impossible to consider the effect of hydrodynamics at its full scale due to limitations of the model). In the case of the single tube calculations the time dependence is $t^{0.5}$.

In the case of the block simulations all curves are characterised by the time dependence $t^{0.6}$. This change is explained by the different levels of concentration near the tube's ends due to accumulation of the solute near the ends outside the tube. In terms of the speed of solute penetration into the tube, the dependence would be $dm/dt \sim t^{-0.4}$ which differs from the experimental observations. The revealed dependence of the dissolution rate on the tube's diameter was also incorrect.

3. Phase-field theory

In the following part, we adopt the phase-field approach to describe the evolution of the solute/solvent mixture. The idea of the approach is to smear the interface, and to use one set of equations for the entire multiphase system, for both phases and the phase boundary. The position of the interface is traced through the gradients of concentration.

The specific free energy function of the binary mixture is defined as follows,

$$f = f_0 + \frac{\epsilon}{2}(\nabla C)^2. \tag{10}$$

Here, the second term accounts for the surface tension effects. The capillary coefficient ϵ is assumed to be so small that the surface tension term can be neglected everywhere except the places of larger concentration gradients, i.e. except the interfaces. The first term, f_0, is the classical part of the free energy, that defines the possible states of the mixture. We are interested in multiphase systems that undergo phase transformations. A convenient description for such a system is given by the function first proposed by Landau for the near-critical states [27],

$$f_0 = a\,(C - C_{cr})^2 + b\,(C - C_{cr})^4\,. \tag{11}$$

Here, C_{cr} is the concentration at the critical point, and a and b are two phenomenological parameters. In the near critical region, parameter a is proportional to the temperature difference from the critical point, $(T \to T_{cr})$, and thus can be negative or positive. The second parameter b is always positive. If a is positive then the equilibrium state of the mixture is homogeneous, and if a is negative then the equilibrium state can be either homogeneous or heterogeneous dependent on the average concentration (the amounts of solvent and solute added to a closed system).

The dissolution process can be viewed as a transformation of a heterogeneous state of a binary mixture to a homogeneous state. In the simplest case, in the absence of hydrodynamic flows, the

time changes of the concentration is defined by the diffusive flux, $\vec{j}$,

$$\frac{\partial C}{\partial t} = -\nabla \cdot \vec{j}. \tag{12}$$

For the Fick's diffusion the diffusive flux is taken to be proportional to the gradient of concentration, $\vec{j} = -D\nabla C$. Such an approach however becomes invalid for the phase boundaries, when the concentration gradients are large [27]. Moreover, for some binary mixtures the equilibrium state may be heterogeneous, i.e. in such a state there is no mass transfer across the boundary despite a strong concentration difference. In equilibrium the chemical potentials of the adjoining phases are equal. Thus, the non-homogeneities in the chemical potential can be used to define the rate of transformation of a system to its thermodynamic equilibrium.

There are two basic models to define the kinetics of the phase transition [28, 29, 30]. In the Landau-Ginzburg model, the rate of the concentration changes is assumed to be proportional to the chemical potential. In the Cahn-Hilliard model, the diffusive flux is taken to be proportional to the gradient of the chemical potential. Both models can be used to define the kinetics of phase transitions of different nature. The Landau-Ginzburg model is however generally applied to the diffusion-less phase transitions (such as the phase transformations in magnetic materials or in liquid crystals [30]). The Cahn-Hilliard model assumes that the order parameter obeys the local conservation law, which is the case for the diffusion process in a binary mixture, when concentration (used as a order parameter) obeys the law of conservation of the species mass [29].

In this work, following the experimental work [1], we restrict our analysis to isothermal systems. It should be mentioned though that phase transformations may frequently involve release or absorption of some latent heats. We are unaware of any experimental measurements of the latent heats for dissolution processes. For the processes of melting and solidification though, the thermal diffusion of the latent heat can define the motion of a liquid/solid boundary [31, 11].

The evolution of the multiphase liquid/liquid binary mixture is defined by the Boussinesq approximation of the the Cahn-Hilliard-Navier-Stokes equations [6],

$$\begin{aligned} \nabla \cdot \vec{v} &= 0, \\ \frac{1}{Pe}\frac{\partial \vec{v}}{\partial t} + (\vec{v}\cdot\nabla)\vec{v} &= -\nabla\Pi + \frac{1}{Re}\nabla^2\vec{v} - C\nabla\mu + 2GrC\vec{\gamma}, \\ \frac{1}{Pe}\frac{\partial C}{\partial t} + (\vec{v}\cdot\nabla)C &= \frac{1}{Pe}\nabla^2\mu. \end{aligned} \tag{13}$$

Here, pressure Π is to be obtained from the compressibility constraint. The equations are written

in non-dimensional form. The scales used for the non-dimensionalisation were, the typical length L_*, the time scale $\tau_* = \rho_* L_*^2/\alpha\mu_*$, the velocity scale $v_* = \mu_*^{1/2}$, the typical density ρ_* (e.g. ρ_1), the typical pressure $\Pi_* = \rho_*\mu_*$, and the typical value of the chemical potential $\mu_* = b$.

The equations include the following non-dimensional parameters. The Reynolds and Peclet numbers,

$$Re = \frac{\rho_* \mu_*^{\frac{1}{2}} L_*}{\eta_*},\ Pe = \frac{\rho_* L_*}{\alpha \mu_*^{\frac{1}{2}}}, \tag{14}$$

where η_* is the typical value of the viscosity coefficient (e.g. ${\eta_1}^2$), and α is the coefficient of mobility. The Grashof number,

$$Gr = \phi \frac{g L_*}{\mu_*},\ \phi = \frac{\rho_2 - \rho_1}{\rho_1}, \tag{15}$$

with ϕ being the density contrast of two liquids. The capillary number[3],

$$Ca = \frac{\epsilon}{\mu_* L_*^2}. \tag{16}$$

Finally, one parameter defines the thermodynamic model for the mixture,

$$A = \frac{a}{b}. \tag{17}$$

The above non-dimensional parameters (14)-(15) are written in terms of the phenomenological parameters introduced within the phase-field approach, such as the capillary and mobility coefficients. The classical names, Peclet, Reynolds, and Grashof numbers, are used to call these parameters, since these numbers appear in front of the corresponding terms of the governing equations (13), and have similar meanings for the analysis of the results. For instance, the Peclet number defines the ratio between the convective and diffusive mass transport. The Grashof number defines the intensity of the convective motion. The Reynolds number defines the viscous force.

[2]Equations (13) assume that the viscosity coefficient may depend on concentration but this dependence is weak, and so may be disregarded if the flows and the non-homogeneities of the velocity field are also small.[6]

[3]This parameter should not be mixed with another classical parameter, also called as the capillary number, and defined as $\eta V/\sigma$, with η, V, and σ being the typical values of viscosity, velocity, and surface tension. The classical capillary number is used in the sharp-interface model to define the ratio between the viscous and capillary forces. The introduced parameter is called the capillary parameter to underline that is proportional to the capillary constant, and hence defines the strengths of the capillary effect. In some papers, e.g. [12], an alternative name, the Cahn number, is also used to call the same parameter.

The expression for the chemical potential μ includes the classical and non-classical parts,

$$\mu = \mu_0 + Gry - Ca\nabla^2 C,\ \mu_0 = \frac{df_0}{dC}. \tag{18}$$

The classical part of the chemical potential, μ_0, is defined from the classical part of the free energy function. The term with Grashof number stands for the effect of barodiffusion (y is the vertical coordinate). The last term in (18) means that the surface energy effects define not only the interface morphology but also the diffusion through the interfacial boundary.

Further, for convenience, the reference point for the field of concentration is shifted, $(C - C_{cr}) \rightarrow C$.

In non-dimensional form the Landau expression (11) reads

$$f_0 = AC^2 + C^4, \tag{19}$$

where the scale of the specific free energy is was taken to be $f_* = \mu_* = b$. Expression (19) works well for the near-critical system, though it tends to produce non-physical values of concentration (i.e. outside the range of concentrations for the pure liquids) for the systems far from the critical point. To get rid of these non-physical values in concentration, the free energy function was modified as follows,

$$f_0 = \frac{3}{4}\left[\left(\frac{1}{2}+C\right)\ln\left(\frac{1}{2}+C\right) + \left(\frac{1}{2}-C\right)\ln\left(\frac{1}{2}-C\right)\right] - \left(\frac{3}{2}-A\right)C^2. \tag{20}$$

The latter function coincides with the Landau expression near the critical point (i.e. when $C \rightarrow 0$) if $C_{cr} = 1/2$. Function (20) also looks similar to the regular-solution expression [9, 10], that is frequently used for the description of the polymerization/de-polymerization processes [32]. For the new function (20), the classical part of the chemical potential reads

$$\mu_0 = \frac{3}{4}\ln\left(\frac{\frac{1}{2}+C}{\frac{1}{2}-C}\right) - (3-2A)C. \tag{21}$$

The governing equations (13) are supplemented with the following boundary conditions. The standard no-slip boundary conditions are imposed for the velocity field. Zero normal derivatives of the chemical potential at the walls reflect the absence of the diffusive flux through the walls. Since the governing equations (13) are of the fourth order in terms of the concentration field, additional conditions are required at the walls. These additional conditions define the wetting properties of the walls. In the current work our analysis is restricted to consideration of two simplified wetting conditions. First, we assume that the solid walls are neutral to the components of the mixture (the

molecules of the solid have the same attraction or repulsion forces with the molecules of the solute and solvent). In that case the contact line is orthogonal to the wall, that is defined by imposing zero normal derivatives of concentration at the walls. Second, we assume that the molecules of the solute, that initially occupies the tube, remain attached to the wall during the whole process of dissolution (that is the molecules of the solid attract the solute molecules much stronger than the molecules of the solvent). The latter boundary condition is mathematically defined by imposing the concentration level at the wall equal to the concentration of the pure solute.

The formulated mathematical model is solved numerically for the $2D$ plane layer and for the $2D$ block geometry. For the numerical solution the equations (13) are rewritten in the vorticity-streamfunction formulation and are solved by using the finite-difference approach.

4. Phase-field results

The concentration fields obtained within the phase-field approach are depicted in figure 2. The dissolution occurs through the propagation of the solute/solvent interfaces into the capillary, as observed in the experiment. The interface can be clearly seen, and the interface has the same thickness during the entire duration of the numerical experiments. In figure 2e the flow vortices attached to the solute/solvent boundaries can be also seen. The vortices are well localised in contrast to the Fickian-based results (figure 1c). The flow amplitude is however much reduced for the case of the solute-philic walls (figure 2f).

The propagation of the interface can still be characterised with the mass of the solvent that enters the tube. In addition, since the interface can now be more accurately positioned, the size of the capillary that is occupied by the solvent phase, L, can be used as another characteristics of the dissolution rate. The latter characteristics was used for the presentation of the experimental results in Ref. [1]. The time evolution of the solvent mass enclosed in the tube and the portion of the tube occupied by the solvent-rich phase are depicted in figure 3. In the case of the single tube calculations the penetration of the solvent into the tube happens with the $t^{0.5}$ time dependence. In the case of the block geometry, the solvent penetration occurs slower, with the different time dependences at the initial and later stages. At the later (longer) state, the time dependence is close to $t^{0.4}$, or in terms of the rate of solute penetration into the tube, $dm/dt\ t^{-0.6}$, which looks closer to the experimental dependence ($t^{-2/3}$). In terms of the size of the solute phase, L, the later time dependence is still however close to $t^{0.5}$.

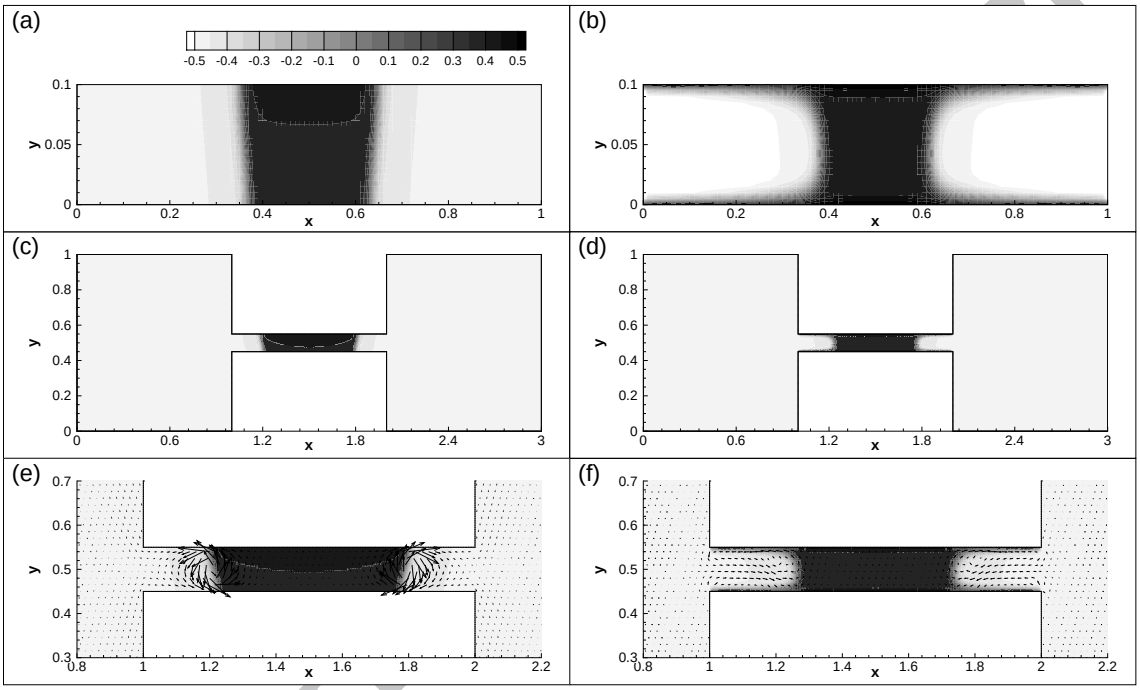

Figure 2: The evolution of the solute/solvent mixture modelled within the phase-field approach. The results are obtained for the neutral (a,c,e) and solute-philic (b,d,f) tube's walls. The snapshots of the concentration and velocity fields at $t = 0.03$ are shown for the single tube (a,b); for the block geometry without hydrodynamics (c,d); and for the block geometry taking into account the hydrodynamic flows (e,f). The results are obtained for $A = -0.5$, $Ca = 10^{-4}$, $Gr = 1$, $Pe = 10^4$, and $Re = 100$ (for (e,f)).

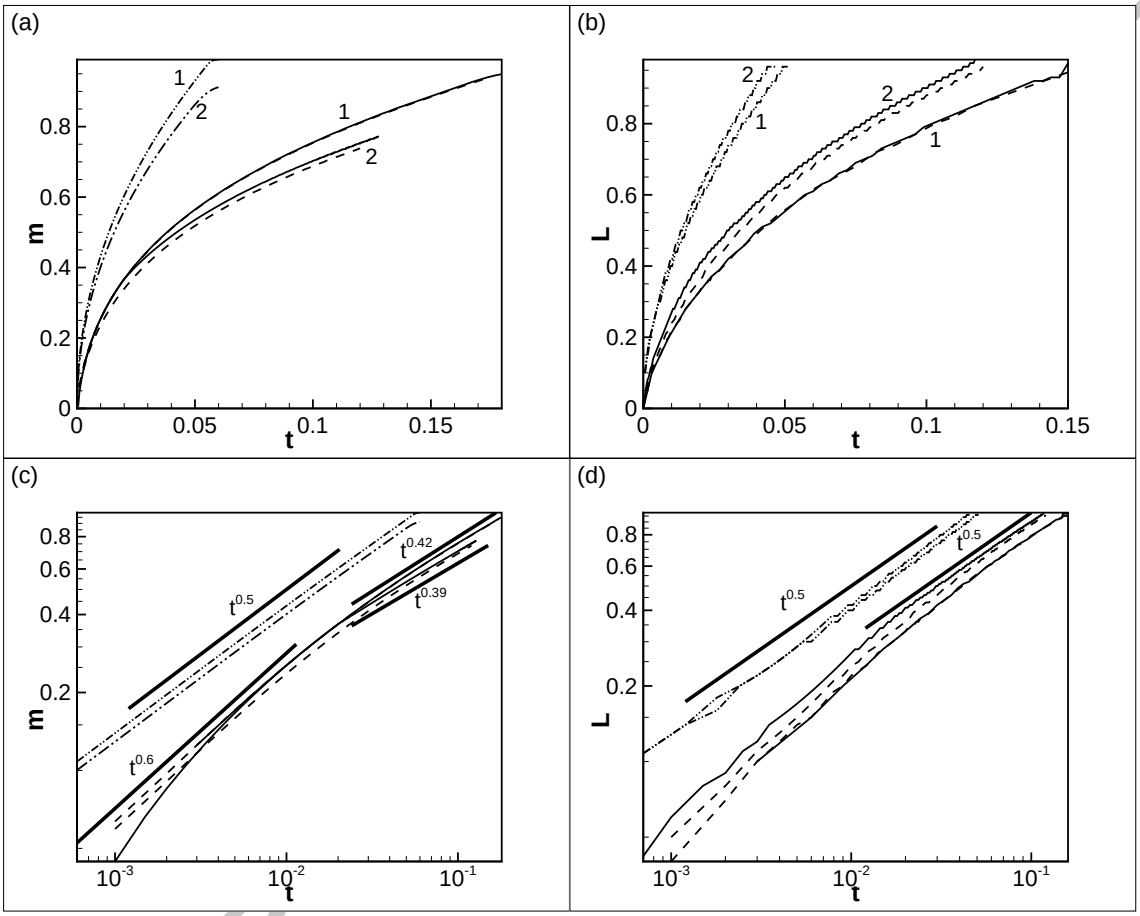

Figure 3: (a) The mass of the solvent penetrating into the tube as a function of time. (b) The portion of the capillary occupied by the solvent phase vs. time. The results are plotted for $d = 0.1$, $A = -0.5$, $Ca = 10^{-4}$, $Gr = 1$, $Pe = 10^4$, and $Re = 100$ (the curves obtained for the cases with the included effects of hydrodynamics). The dash-dot-dot lines depict the results for the single tubes; the dashed lines for the block geometry without hydrodynamics; and the solid lines for the block geometry with hydrodynamics. The lines marked by '1' correspond to the results obtained for the neutral walls, and the lines with '2' correspond to the results with the solute-philic walls. (c,d) The results shown in (a) and (b) but in logarithmic coordinates. The thick lines show the reference dependences.

The results of the phase-field simulations could be correlated with the Fick's model, if the dimensional diffusion coefficient is defined as

$$D_{pf} = \frac{\alpha\mu_*}{\rho_*}\frac{d\mu_0}{dC} = \frac{\alpha\mu_*}{\rho_*}\left(\frac{3/4}{1/4 - C^2} - (3 - 2A)\right). \tag{22}$$

The so-defined diffusion coefficient does not take into account the Cahn-Hilliard addition to the chemical potential, and thus it is negative at $C \sim 0$ (i.e. within the interface zones) if $A < 0$. The Cahn-Hilliard addition makes the overall diffusion coefficient positive within the interface zones, and this is why this addition was introduced. Far from interfaces, D_{pf} can be used as the diffusion coefficient in either solute or solvent phases. The coefficient is concentration-dependent, with growing values when $|C| \to 1/2$. In general, expression (22) produces greater values for the diffusion coefficients in the solvent and solute phases (in comparison with the ones obtained from for the formula (2)). This explains that the dissolution seems to occur faster in the case of the phase-field simulations.

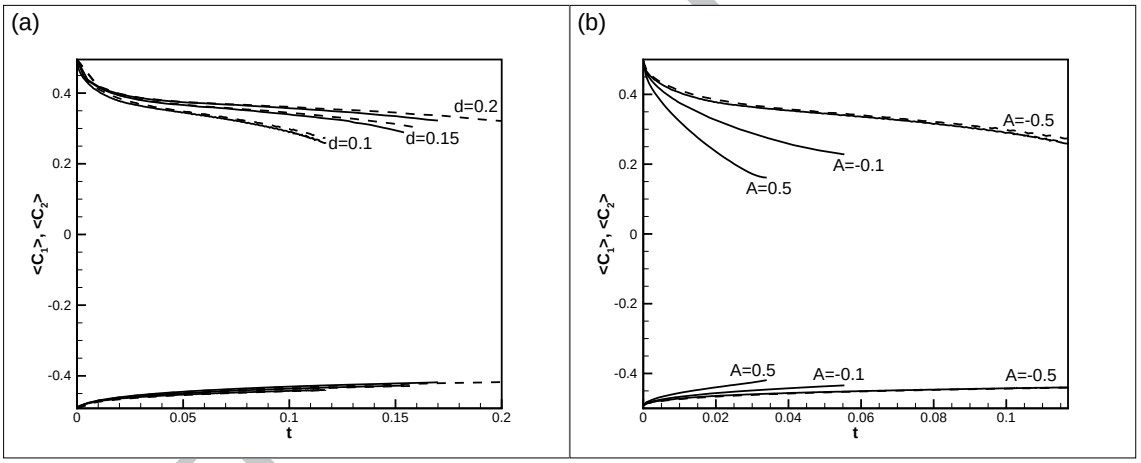

Figure 4: The average concentrations within the solute ($< C_1 >$) and solvent ($< C_2 >$) phases vs. time. The data is obtained from the block geometry calculations for $Gr = 1$, $Ca = 10^{-4}$, $Pe = 10^4$ and (a) $A = -0.5$ and three different diameters of the tube (0.1, 0.15, and 0.2); (b) $d = 0.1$ and three different A (-0.5, -0.1, and 0.5). The dashed lines correspond to the results without the effect of hydrodynamics and the solid lines with the hydrodynamic flows.

Figure 4 depicts the average concentrations within the solute-rich and solvent-rich phases. At initial point, two pure liquids, with the concentrations $C = \pm 1/2$, are brought into contact, which initiates the process of mixing. During the mixing, the concentration levels change so to approach

the equilibrium levels, which are $\approx \pm 0.388$ for the chemical potential defined by equation (21) at $A = -0.5$. One sees that, if A is negative, there is a short initial period ($t \leq 0.01$) when the value of the average concentration in the solute phase quickly adjusts its equilibrium level. The average concentration within the solute domain remains almost constant after that. Such a behaviour agrees with the scenario used for modelling of the dissolution process by Ugrozov et al. [21]. This rapid initial quench also makes the diffusion within the solute phase slower over the main duration of the process (which is similar to the assumption made for the Fickian calculations).

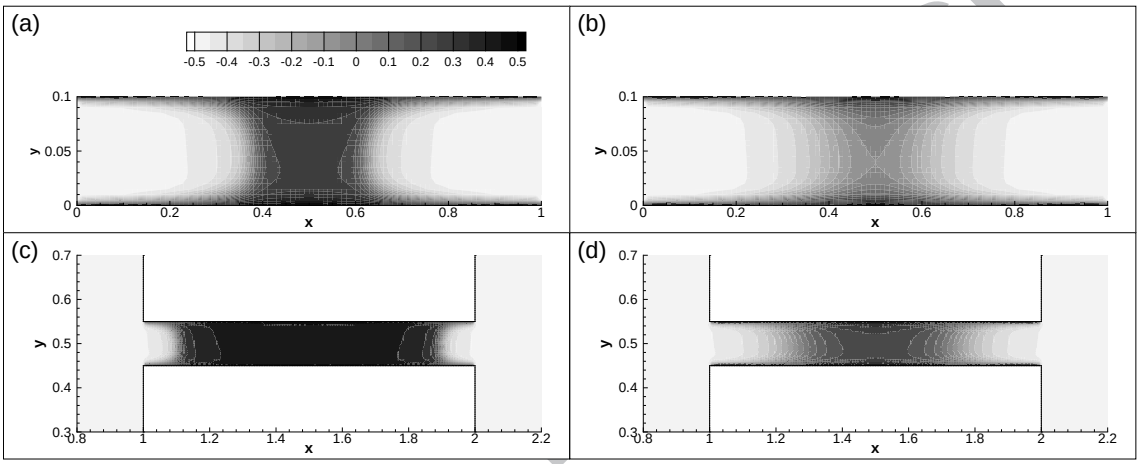

Figure 5: The snapshots of the concentration fields for $d = 0.1$, $Ca = 10^{-4}$, $Gr = 1$, and for (a,c) $A = -0.1$ and (b,d) $A = 0.5$. The time moment is 0.024 in all pictures. In (a,b) the results are shown for the single tube, and in (c,d) for the block geometry.

The shape and the speed of propagation of the solute/solvent boundaries in general depend on all non-dimensional parameters of the phase-field theory. Thus, the thickness of the interface is a strong function of the capillary number and parameter A (figure 5). For the negative values of A, the interface thickness is well defined by the formula for a flat interfacial boundary, $\delta = \sqrt{-Ca/A}$. For the positive values of A the interface becomes even more diffusive, generally resembling the images obtained for the Fickian results. The dissolution occurs much faster for higher values of A that can be seen in figure 7.

The value of the capillary number defines the surface tension associated with the interface (for a flat interface, the coefficient of the surface tension is proportional to $\sqrt{Ca}$). The balance of the capillary and gravity forces are to define the shape of the solute/solvent boundary. We however

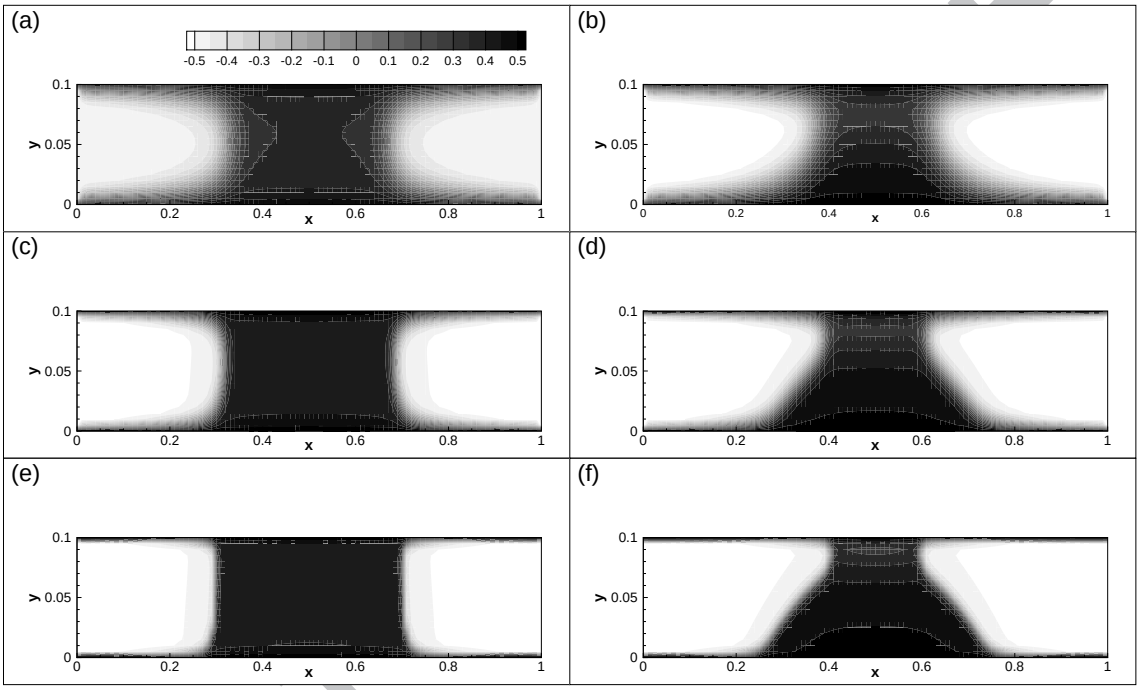

Figure 6: The snapshots of the concentration fields for $d = 0.1$, and three different capillary numbers, $Ca = 4 \cdot 10^{-4}$ (a,b), $Ca = 10^{-4}$ (c,d), and $Ca = 2.5 \cdot 10^{-5}$ (e,f), and two different Grashof numbers, $Gr = 2$ (a,c,e) and $Gr = 10$ (b,d,f). The time moment is 0.02 in all pictures.

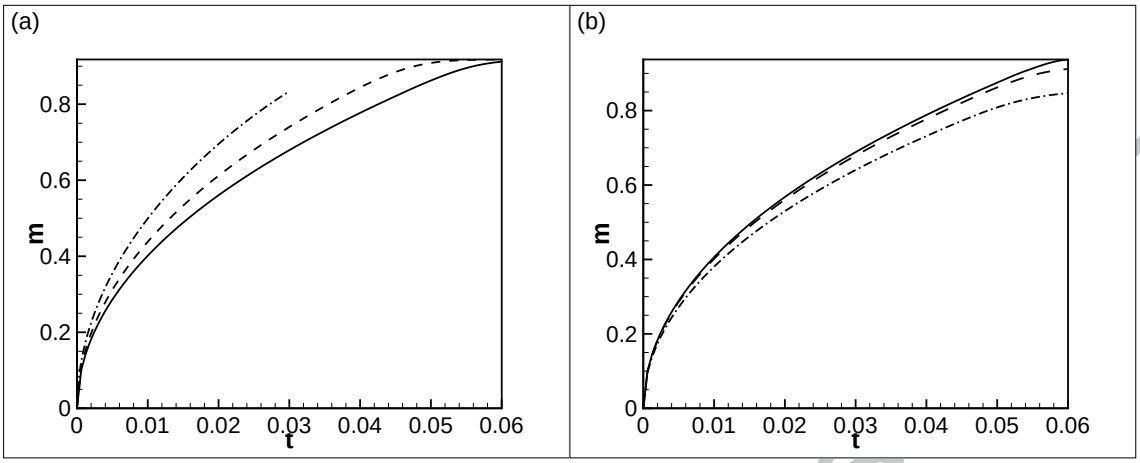

Figure 7: The mass of the solvent within the tube vs. time. The results are obtained for the single tube, (a) for $Ca = 10^{-4}$ and three different A, $A = -0.5$ (solid line), $A = -0.1$ (dashed line), and $A = 0.5$ (dash-dot line); and (b) for $A = -0.5$, and three different Ca, $Ca = 4 \cdot 10^{-4}$ (dash-dot line), $Ca = 10^{-4}$ (dashed line), and $Ca = 2.5 \cdot 10^{-5}$ (solid line).

found that a four-fold reduction in Ca from e.g. figure 6d to figure 6f does not change the interface inclination. The rate of interface propagation is also just slightly affected with the change of the capillary number (see figure 7b). Moreover, the curves obtained for the gradually reducing capillary numbers converge, so revealing the behaviour of an interface of zero thickness.

We also studied how gravity (the density contrast) affects the shape of the interface and the rate of dissolution. In figures 6 and 8a,c the results are shown for the positive values of the Grashof number, but, obviously, the results are symmetrical in respect to the sign of the Grashof number. The interface is getting stronger inclined at larger Grashof numbers. The definition of the Grashof number in the classical (9) and phase-field (15) theories are different, and thus the values used for the calculations are very different. In the case of the Fickian-based calculations the value of the Grashof number was estimated based on the data for the phenomenological parameters. In the case of the phase-field simulations, the values of the introduced phenomenological parameters are not known, and such values could be understood through the comparison of the theoretical and experimental data. Thus, the value of the Grashof number can be derived from the analysis of the interface shape, since only for the Grashof numbers of the order of 1, the obtained interface shapes are similar to the ones observed in the experiments [1]. For the rate of dissolution, one sees that

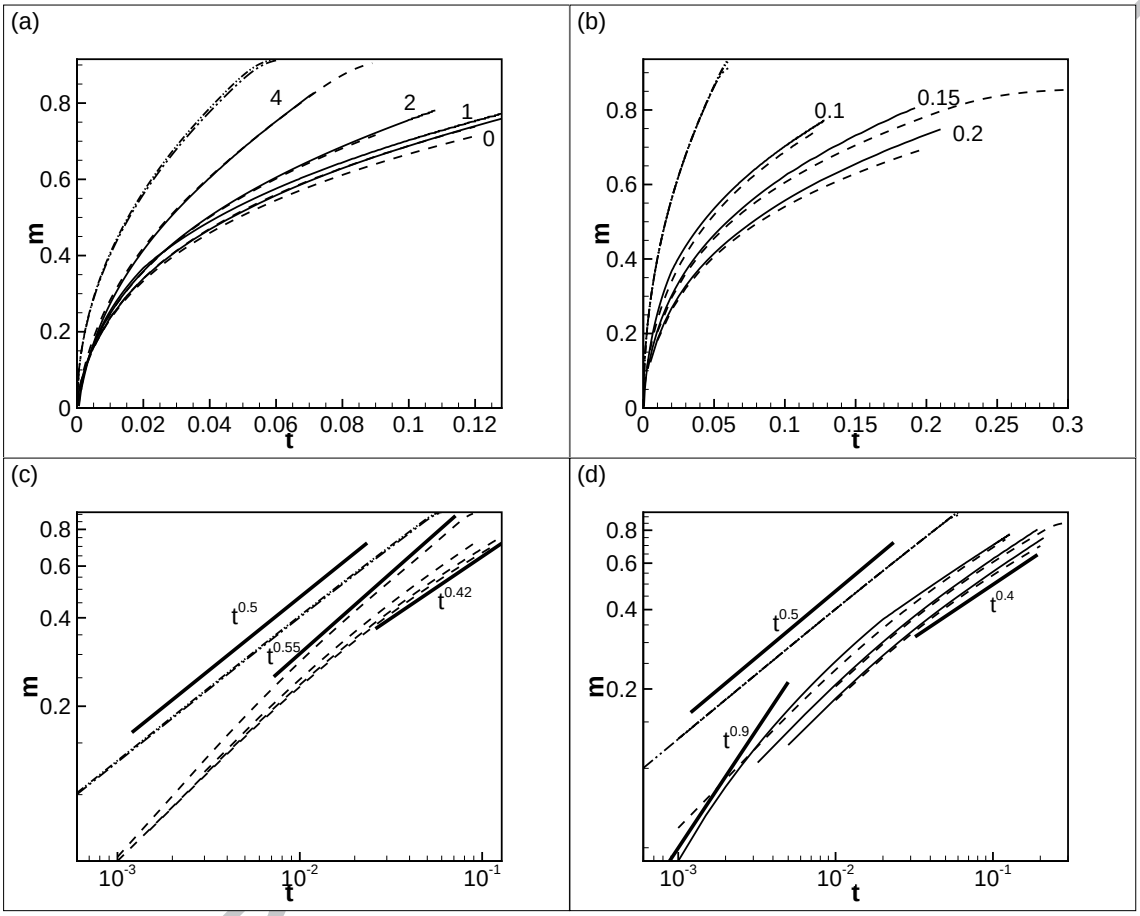

Figure 8: (a) The mass of the solvent penetrating into the capillary as a function of time. The dash-dot-dot lines depict the data obtained for the single tube; the dashed lines show the data for the block geometry with no flows; and the solid lines for the block geometry with flows. (a) The shown curves are obtained for $Gr = 0$, $Gr = 1$, $Gr = 2$, and $Gr = 4$, as indicated in the picture. The lines for the single tube almost coincide. (b) The curves are shown for the different tube diameters, $d = 0.1$, $d = 0.015$, and $d = 0.2$, as shown in the picture. The lines for the single tube coincide. (c,d) The same data as in (a) and (b) are shown in the logarithmic coordinates. Although in (c) only the results for the pure diffusion calculations are shown for clarity.

stronger gravity means faster dissolution (see figure 8a). Since, the contribution of hydrodynamic flows in the dissolution is minimal, an increase in gravity results in the stronger barodiffusion effect, that leads to faster interchange of molecules across the solute/solvent boundary. The time dependences of the dissolution curves slightly depend on the Grashof number as shown in figure 8c.

We also found that the change in the results is minimal if the value of the Reynolds number is changed (the range of considered Reynolds numbers was very large, $10^{-9}..10^{9}$), which only underlines that the dissolution is purely defined by diffusion at the parameters used for the simulations.

Finally, we investigated how the dissolution rates are affected by the change of the tube's diameter (figure 8b). We found that the results are rather similar to the observations produced for the Fick's case. For the case of diffusion in a single capillary, the dependence on the tube's diameter is negligible. In the blocks, the dissolution in smaller tubes occurs faster, which contradicts to the experimental observations. The results for the block geometry would approach the data obtained for the single tubes if the tubes are thinner. One can also see that for thinner tubes the two stages with different dependences could be identified, with the latter dependence still close to $t^{0.4}$.

5. Conclusions

'Mixing' is frequently used to refer to the development of various hydrodynamic instabilities, when there is only one fluid (as in the majority of the studies on the shear flow instability), or there are two immiscible liquids (as frequently assumed in the works on the Rayleigh-Taylor instability). There are some exceptions though, for instance, the linear stability of slowly miscible interfaces was studied in Refs. [33, 34].

The current work is focused on the diffusion dynamics of the boundary separating two miscible liquids. The evolution of such systems is frequently modelled on the basis of the Fick's law, which however does not agree with numerous experimental observations (see review [7] for references). In particular, the optical observations of the diffusive evolution of two different liquids enclosed in a capillary are reported in Ref. [1]. In the current study, these experimental results are used to verify the existent theoretical models. Two models were considered, the first model is based on the classical Fick's law, and another advanced model is based on the generalised Fick's law with the account of the capillary effects (the phase-field model). Our comparisons were primarily focused on the shape of the solute/solvent boundary (an inclined boundaries were experimentally observed confirming that a miscible interface should be endowed with some surface tension, and

also suggesting that gravity effects are important even within the capillary) and on the interface dynamics (in the experiments, the interfaces were moving with the speeds significantly exceeding the rate of diffusive smearing).

We found that the Fickian model is not capable of reproducing the experimentally observed shapes of the interfaces, and, moreover, the interfaces are too diffusive, even when the diffusion coefficients of the mixture components are very different. The phase-field simulations reproduce the sharp solute/solvent boundary clearly identifiable during the entire process of dissolution. The boundary thickness however remains constant, while in the experiment the interface was slowly smearing. The boundary is endowed with some surface tension, and its shape could be made very similar to the experimental images. We found that the shape (inclination) of the boundary is predominately defined by the Grashof number. The values of the non-dimensional parameters used in the phase-field approach are generally difficult to define, since their definitions involve the new phenomenological parameters. The comparison of the simulated and experimentally-observed interfaces can be used to say that for the considered system the Grashof number is of order of 1.

The major difficulty of the Fickian and phase-field theories is the prediction of the diffusion rate through the solute/solvent boundary. In the experiment the $t^{-2/3}$-dependence was persistently observed for the speed of the interface propagation into the tube. In the numerical simulations fulfilled for the single tubes we observed the $t^{-1/2}$ time dependence. For the block geometry, the time dependence was different, with the powers close to -0.4 in the Fickian simulations and even close -0.6 for the phase-field simulations. In the case of the phase-field simulations two stages of the dissolution could be also identified, which is also similar to the experiment. Neither approach though reproduces the experimentally-observed dependence of the speed of the solute/solvent boundary on the tube's diameter. In the experiment the dissolution occurred slower in smaller tubes, with the speed proportional to d^2 (d is the tube's diameter). This was never observed in the numerical simulations, where the rate of dissolution is either is independent of the tube's diameter, or even increases in the tubes of smaller diameters.

In this sense, the work remains incomplete. We showed that Fick's theory could not reproduce the dissolution behaviour of a miscible interface between two liquids. This result was expected. The phase-field theory, despite of being capable of accurate modelling of the interface shape, remains incapable of reproducing all features of the interfacial diffusion. Further improvement of the theory is still required to understand the dissolution process in liquid/liquid binary mixtures. In conclusion,

we would like to discuss two possible directions of this work.

One is to investigate whether non-isothermal effects, that might appear from the latent heat of dissolution, could affect the propagation of the solute/solvent boundary. As noted in the introduction, such effects frequently define the motion of the solidification and melting fronts, which have many features similar to the observations for the solute/solvent interfaces.

Another direction is to extend the phenomenological relations accepted here for the diffusion flux and the viscous stress tensor. These two quantities are defined by the gradient of the chemical potential, and by the gradients of the velocity components. Both expressions are written in assumption that the medium is isotropic. In the phase-field theory, an interface (strong gradients in concentration field) introduces anisotropy, so the classical relations between the thermodynamic fluxes and forces should in general be reconsidered. This makes possible to assume that the diffusion flux is driven by both gradients of the chemical potential and velocity, and the viscous stress tensor in turn is defined by the non-homogeneities in velocity field and by the gradient of the chemical potential [35]. A theory with similar ideas was constructed for the polymerisation/de-polymerisation process [36], that is also mainly described by diffusion through the monomer/polymer boundary, and where non-Fickian dependences are regularly observed. The non-Fickian diffusion of the polymerization front was reproduced on the basis of the extended phenomenological relations between the thermodynamic fluxes and forces.

6. Acknowledgments

The authors gratefully acknowledge financial support from the Government of Perm region, Russia (Contract No. C-26-0004.3).

7. References

References

[1] M. S. Stevar, A. Vorobev, Shapes and dynamics of miscible liquid/liquid interfaces in horizontal capillary tubes, Journal of Colloid and Interface Science 383 (1) (2012) 184 – 197.

[2] D. Jacqmin, Calculation of two-phase navier-stokes flows using phase-field modeling, Journal of Computational Physics 155 (1999) 96–127.

[3] L. P. Csernai, J. I. Kapusta, E. Osnes, Domain wall dynamics of phase interfaces, Phys. Rev. D 67 (2003) 045003.

[4] N. Moelans, B. Blanpain, P. Wollants, An introduction to phase-field modeling of microstructure evolution, Calphad 32 (2) (2008) 268 – 294.

[5] B. Nestler, A. Choudhury, Phase-field modeling of multi-component systems, Current Opinion in Solid State and Materials Science 15 (3) (2011) 93 – 105.

[6] A. Vorobev, Boussinesq approximation of the cahn-hilliard-navier-stokes equations, Phys. Rev. E 82 (2010) 056312.

[7] A. Vorobev, Dissolution dynamics of miscible liquid/liquid interfaces, Current Opinion in Colloid and Interface Science 19 (2014) 300–308.

[8] D. D. Joseph, Y. Y. Renardy, Fundamentals of two-fluid dynamics. Pt. II: Lubricated transport, drops and miscible liquids, Springer-Verlag, 1993.

[9] J. W. Cahn, J. E. Hilliard, Free energy of a nonuniform system. i. interfacial free energy, The Journal of Chemical Physics 28 (2) (1958) 258–267.

[10] J. W. Cahn, J. E. Hilliard, Free energy of a nonuniform system. iii. nucleation in a twocomponent incompressible fluid, The Journal of Chemical Physics 31 (3) (1959) 688–699.

[11] A. Umantsev, Thermal effects in dynamics of interfaces, The Journal of Chemical Physics 116 (10) (2002) 4252–4265.

[12] J. Lowengrub, L. Truskinovsky, Quasi-incompressible cahn-hilliard fluids and topological transitions, Royal Society of London Proceedings Series A 454 (1998) 2617–2654.

[13] C.-Y. Chen, E. Meiburg, Miscible displacements in capillary tubes. part 2. numerical simulations, Journal of Fluid Mechanics 326 (1996) 57–90.

[14] C.-Y. Chen, E. Meiburg, Miscible displacements in capillary tubes: Influence of korteweg stresses and divergence effects, Physics of Fluids 14 (7) (2002) 2052–2058.

[15] D. Wilhelm, E. Meiburg, Three-dimensional spectral element simulations of variable density and viscosity, miscible displacements in a capillary tube, Computers & Fluids 33 (3) (2004) 485 – 508.

[16] N. Bessonov, J. A. Pojman, V. Volpert, Modelling of diffusive interfaces with temperature gradients, Journal of Engineering Mathematics 49 (2004) 321–338.

[17] J. A. Pojman, Y. Chekanov, V. Wyatt, N. Bessonov, V. Volpert, Numerical simulations of convection induced by korteweg stresses in a miscible polymer-monomer system: Effects of variable transport coefficients, polymerization rate and volume changes, Microgravity Sci. Technol. 21 (2009) 225–237.

[18] J. A. Pojman, C. Whitmore, M. L. T. Liveri, R. Lombardo, J. Marszalek, R. Parker, B. Zoltowski, Evidence for the existence of an effective interfacial tension between miscible fluids: isobutyric acid-water and 1-butanol-water in a spinning-drop tensiometer, Langmuir 22 (6) (2006) 2569–77.

[19] G. Viner, J. A. Pojman, Studying diffusion of partially miscible and systems near their consolute point by laser line deflection, Optics and Lasers in Engineering 46 (12) (2008) 893 – 899.

[20] D. Antrim, P. Bunton, L. L. Lewis, B. D. Zoltowski, J. A. Pojman, Measuring the mutual diffusion coefficient for dodecyl acrylate in low molecular weight poly(dodecyl acrylate) with laser line deflection (wiener's method) and the fluorescence of pyrene, J. Phys. Chem B 109 (2005) 11842.

[21] V. Ugrozov, A. Filippov, C. Paraskeva, G. Constantinides, V. Starov, Diffusive dissolution of a drop in a capillary, Colloids and Surfaces A: Physicochemical and Engineering Aspects 239 (13) (2004) 129 – 133.

[22] J. W. Jawitz, M. D. Annable, P. Rao, Miscible fluid displacement stability in unconfined porous media: Two-dimensional flow experiments and simulations, Journal of Contaminant Hydrology 31 (34) (1998) 211 – 230.

[23] V. Alvarado, E. Manrique, Enhanced oil recovery: An update review, Energies 3 (2010) 1529–1975.

[24] M. Sohrabi, M. Riazi, M. Jamiolahmady, N. I. Kechut, S. Ireland, G. Robertson, Carbonated water injection (cwi) a productive way of using co2 for oil recovery and co2 storage, Energy Procedia 4 (0) (2011) 2192 – 2199.

[25] M. L. M. N. Cerutti, A. A. U. de Souza, S. M. d. A. G. U. de Souza, Solvent extraction of vegetable oils: Numerical and experimental study, Food and Bioproducts Processing 90 (2) (2012) 199 – 204.

[26] P. Petitjeans, T. Maxworthy, Miscible displacements in capillary tubes. part 1. experiments, Journal of Fluid Mechanics 326 (1996) 37–56.

[27] L. D. Landau, E. M. Lifshits, L. P. Pitaevskii, Statistical Physics. Course of theoretical physics, Pergamon Press, 1980.

[28] H. Metiu, K. Kitahara, J. Ross, Stochastic theory of the kinetics of phase transitions, The Journal of Chemical Physics 64 (1) (1976) 292–299.

[29] H. Metiu, K. Kitahara, J. Ross, A derivation and comparison of two equations (landauginzburg and cahn) for the kinetics of phase transitions, The Journal of Chemical Physics 65 (1) (1976) 393–396.

[30] S. Chan, Steadystate kinetics of diffusionless first order phase transformations, The Journal of Chemical Physics 67 (12) (1977) 5755–5762.

[31] J. S. Langer, Instabilities and pattern formation in crystal growth, Reviews of Modern Physics (1) (1980) 1–30.

[32] P. J. Flory, Principles of polymer chemistry, Cornell University Press, Ithaca, New York, 1953.

[33] A. Kheniene, A. Vorobev, Linear stability analysis of a horizontal phase boundary separating two miscible liquids, Phys. Rev. E 88 (2013) 022404 (15pp).

[34] A. Kheniene, A. Vorobev, Linear stability of a horizontal phase boundary subjected to shear motion, Eur. Phys. J. E 38 (2015) 77 (12pp).

[35] A. B. Roshchin, L. M. Truskinovskii, Model of a weakly non-local relaxing compressible medium, PMM U.S.S.R. 53 (1989) 715–720.

[36] D. S. Cohen, A. B. White, Sharp fronts due to diffusion and viscoelastic relaxation in polymers, SIAM J. Appl. Math. 51 (1991) 472–483.

Graphical Abstract